Anomalous Metamagnetism in the Low Carrier Density Kondo Lattice $YbRh_3Si_7$

Binod K. Rai,[1] S. Chikara,[2] Xiaxin Ding,[2] Iain W. H. Oswald,[3] R. Schönemann,[4] V. Loganathan,[1] A. M. Hallas,[1] H. B. Cao,[5] Macy Stavinoha,[6] T. Chen,[1] Haoran Man,[1] Scott Carr,[1] John Singleton,[2] Vivien Zapf,[2] Katherine A. Benavides,[3] Julia Y. Chan,[3] Q. R. Zhang,[4] D. Rhodes,[4] Y. C. Chiu,[4] Luis Balicas,[4] A. A. Aczel,[5] Q. Huang,[7] Jeffrey W. Lynn,[7] J. Gaudet,[8] D. A. Sokolov,[9] H. C. Walker,[10] D. T. Adroja,[10] Pengcheng Dai,[1] Andriy H. Nevidomskyy,[1] C.-L. Huang,[1,*] and E. Morosan[1]

[1]*Department of Physics and Astronomy, Rice University, Houston, Texas 77005, USA*
[2]*National High Magnetic Field Laboratory, Materials Physics and Applications Division, Los Alamos National Laboratory, Los Alamos, New Mexico 87545, USA*
[3]*Department of Chemistry and Biochemistry, University of Texas at Dallas, Richardson, Texas 75080, USA*
[4]*National High Magnetic Field Laboratory, Florida State University, Tallahassee, Florida 32310, USA*
[5]*Neutron Scattering Division, Oak Ridge National Laboratory, Oak Ridge, Tennessee 37831, USA*
[6]*Department of Chemistry, Rice University, Houston, Texas 77005, USA*
[7]*NIST Center for Neutron Research, National Institute of Standards and Technology, Gaithersburg, Maryland 20899, USA*
[8]*Department of Physics and Astronomy, McMaster University, Hamilton, Ontario L8S 4M1, Canada*
[9]*Max Planck Institute for Chemical Physics of Solids, Dresden, 01187 Germany*
[10]*ISIS Facility, Rutherford Appleton Laboratory, Harwell Campus, Didcot, OX11 0QX, United Kingdom*

(Received 10 March 2018; revised manuscript received 26 September 2018; published 13 December 2018)

We report complex metamagnetic transitions in single crystals of the new low carrier Kondo antiferromagnet $YbRh_3Si_7$. Electrical transport, magnetization, and specific heat measurements reveal antiferromagnetic order at $T_N = 7.5$ K. Neutron diffraction measurements show that the magnetic ground state of $YbRh_3Si_7$ is a collinear antiferromagnet, where the moments are aligned in the ab plane. With such an ordered state, no metamagnetic transitions are expected when a magnetic field is applied along the c axis. It is therefore surprising that high-field magnetization, torque, and resistivity measurements with $H\|c$ reveal two metamagnetic transitions at $\mu_0 H_1 = 6.7$ T and $\mu_0 H_2 = 21$ T. When the field is tilted away from the c axis, towards the ab plane, both metamagnetic transitions are shifted to higher fields. The first metamagnetic transition leads to an abrupt increase in the electrical resistivity, while the second transition is accompanied by a dramatic reduction in the electrical resistivity. Thus, the magnetic and electronic degrees of freedom in $YbRh_3Si_7$ are strongly coupled. We discuss the origin of the anomalous metamagnetism and conclude that it is related to competition between crystal electric-field anisotropy and anisotropic exchange interactions.

DOI: 10.1103/PhysRevX.8.041047

Subject Areas: Condensed Matter Physics, Magnetism, Strongly Correlated Materials

I. INTRODUCTION

Materials containing partially filled f orbitals are of great interest to the strongly correlated electron system community because of their quantum complexity. This is driven by several competing parameters that include Kondo coupling (which favors a nonmagnetic ground state with enhanced effective mass), Rudermann-Kittel-Kasuya-Yosida interactions (RKKY, which favor long-range magnetic order), and crystal electric-field (CEF) effects (which lift the degeneracy of the Hund's rule ground-state multiplet). Among f-electron systems, the ground states of many Ce-, Yb-, and U-based compounds are highly susceptible to tuning by nonthermal control parameters, such as pressure, chemical substitution, or magnetic field [1]. This often results in emergent phenomena, with unconventional superconductivity [2–4], non-Fermi liquid behavior near a quantum critical point [3,5–9], hidden order [4], and metamagnetism being just a few prominent examples [10–18]. In several materials, metamagnetism has been linked with magnetic quantum criticality [16,19], although the origin is unclear.

Here, we report the discovery of metamagnetism in single crystals of the Kondo lattice $YbRh_3Si_7$. $YbRh_3Si_7$ is the first compound displaying either Kondo correlations or metamagnetism in the $ScRh_3Si_7$ (1-3-7) family [20,21], for

*clh@rice.edu

which the only known rare earth-based systems are nonmagnetic $R\mathrm{Au_3Al_7}$ (R = Ce-Sm, Gd-Lu) [22], magnetic $\mathrm{Eu(Rh,Ir)_3Ge_7}$ [23], and $\mathrm{YbAu_3Ga_7}$ with unknown physical properties [24]. In $\mathrm{YbRh_3Si_7}$, the Kondo effect is clearly indicated by Kondo latticelike resistivity, reduced magnetic entropy released at an antiferromagnetically ordered temperature T_N, and density functional theory (DFT) calculations. Anisotropic magnetic susceptibility and specific heat measurements reveal long-range magnetic order below $T_N = 7.5$ K. Neutron diffraction measurements confirm that the zero field ordered state is antiferromagnetic (AFM), with the moments lying in the ab plane.

We present high-field magnetization, torque, and resistivity up to 35 T. Around 2 K, these measurements reveal two field-induced metamagnetic (MM) transitions at $\mu_0 H_1 = 6.7$ T and $\mu_0 H_2 = 21$ T along the c axis. Angle-dependent magnetoresistivity shows that both H_1 and H_2 increase monotonically when the crystal is rotated away from the c axis towards the ab plane. When $H \perp c$, only one MM transition is found, up to the maximal field, at $\mu_0 H_1 = 10$ T. This behavior is starkly different from what has been observed in other $4f$- and $5f$-based MM materials; MM transitions are rarely observed for a field orthogonal to the moments and, if present, typically occur at higher fields than those for the field parallel to the moments [10–18,25–37]. Given that the easy axis, determined by the CEF anisotropy, is along the c axis, while the ordered moment is lying in the ab plane, the anomalous metamagnetism in $\mathrm{YbRh_3Si_7}$ may be a result of the delicate balance among different underlying energy scales, including CEF anisotropy and exchange anisotropy. Understanding the metamagnetism in $\mathrm{YbRh_3Si_7}$ will help draw a more complete picture of how subtle quantum effects steer the macroscopic behavior of different materials.

II. METHODS

Single crystals of $\mathrm{YbRh_3Si_7}$ were grown from a Rh-Si excess liquid solution using Yb (99.9999%), Rh (99.95%), and Si (99.99%). The mixture was slowly cooled from 1200 °C to 1100 °C, and when the excess flux was decanted, rhombohedral crystals with typical dimensions of 3–5 mm were obtained. The as-grown single crystals were subsequently annealed up to 200 hours under partial Ar atmosphere at 850 °C.

Room-temperature powder x-ray diffraction patterns were collected in a Bruker D8 diffractometer using Cu Kα radiation, and the patterns were refined using the TOPAS software. Additional single-crystal diffraction measurements were performed in a Bruker D8 Quest Kappa diffractometer equipped with an IμS microfocus source ($\lambda = 0.71073$ Å) operating at 50 kV and 1 mA, a HELIOS optics monochromator, and a CMOS detector. The crystal structure of $\mathrm{YbRh_3Si_7}$ was solved using direct methods in SHELXS2013 (Ref. [38]), and all atomic sites were refined anisotropically using SHELXL2014 (Ref. [39]) (see Table S1 and S2 in Ref. [40]). Powder neutron diffraction data were collected on the BT-1 high-resolution neutron powder diffractometer and on the BT-7 triple-axis diffractometer at the NIST Center for Neutron Research. We used an (002) pyrolytic graphite (PG) crystal as a monochromator, with an incident beam energy of 14.7 meV and a PG filter to suppress higher-order wavelength contaminations. Coarse collimations of Open-80-80 Radial collimations (FWHM) were employed, with a position-sensitive detector [41]. Single-crystal neutron diffraction in zero magnetic field was performed on the four-circle diffractometer HB-3A at the High Flux Isotope Reactor (HFIR) at Oak Ridge National Laboratory (ORNL). The data were collected at 4 K and 15 K by neutrons with a wavelength of 1.546 Å from a bent perfect Si (220) monochromator [42]. Single-crystal neutron diffraction, with a magnetic field applied parallel to the c axis, was performed on the fixed incident energy triple-axis HB-1A at HFIR ($\lambda = 2.36$ Å). A selection of Bragg peaks in the (HK0) scattering plane was measured at 1.8 K and 10 K in fields up to 8 T. The magnetic symmetry analysis was performed with SARAh [43]. The nuclear and magnetic structure refinements were carried out with the FullProf Suite [44]. Inelastic neutron scattering experiments were carried out using the MERLIN neutron chopper spectrometer at ISIS, UK [45].

Anisotropic temperature- and field-dependent dc magnetization measurements were done in a Quantum Design (QD) Magnetic Property Measurement System (MPMS) with a ^{3}He option. Specific heat data were collected in a QD Physical Property Measurement System (PPMS) and a Dynacool with a dilution refrigerator using a thermal relaxation method for temperatures between 0.05 K and 30 K and magnetic fields up to 9 T. The temperature-dependent ac resistivity of bar-shaped crystals was collected in the QD PPMS, with $f = 17.77$ Hz and current $i = 1$ mA parallel to the c axis using a standard four-terminal configuration.

To elucidate the electronic and magnetic properties of $\mathrm{YbRh_3Si_7}$, band-structure calculations were performed using DFT with the linearized augmented plane waves as a basis, as implemented in the WIEN2K code [46]. The generalized gradient approximation was used to account for the exchange and correlations [47], and the polyhedron integration method was used to calculate the electronic density of states (DOS). The effect of Hubbard U was incorporated within the DFT + U method [48].

The high-field magnetization measurements up to 35 T were performed using an extraction magnetometry technique in a capacitor-driven pulsed field magnet at the pulsed field facility at Los Alamos National Laboratory. The change in magnetization, ΔM with magnetic field H, was obtained by integrating the induced voltage with the sample inside a compensated coil and subtracting the integrated voltage recorded in a subsequent sample-out

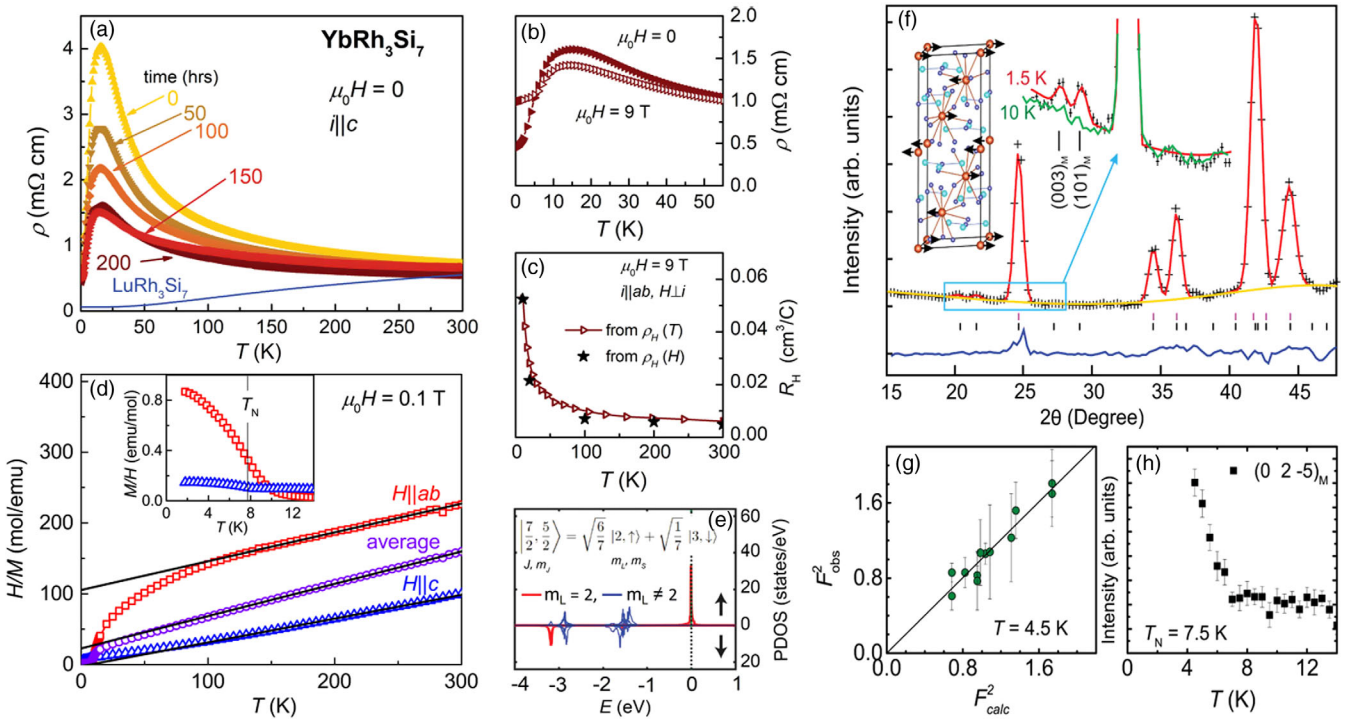

FIG. 1. (a) Zero-field temperature-dependent electrical resistivity ρ of $YbRh_3Si_7$ at different annealing times. The solid line is the data for $LuRh_3Si_7$. (b) Low-temperature ρ at $\mu_0 H = 0$ and 9 T applied parallel to the c axis. (c) Hall coefficient R_H measured at $\mu_0 H = 9$ T between 300 and 10 K. (d) Inverse magnetic susceptibility H/M vs T for $YbRh_3Si_7$ with $\mu_0 H = 0.1$ T parallel to c (blue triangles) and ab (red squares) together with a polycrystalline average (purple circles) and Curie-Weiss fits (solid lines). Inset: Low-temperature magnetic susceptibility M/H. Note that 1 emu = 1 G cm^3 = 10^{-3} Am^2. (e) DOS projected onto the orbital angular-momentum components of the Yb^{3+} ion. (f) Powder neutron diffraction patterns at 1.5 K (data, crosses; Bragg peak positions, short vertical lines; difference between data and refined pattern, indigo curve), with the AFM structure of the system with collinear moments parallel to the a axis (left inset) and an enhanced view of the (0 0 3) and (1 0 1) magnetic Bragg peaks at small angles (right inset). (g) Agreement of the single-crystal magnetic structure refinement at $T = 4.5$ K. (h) Magnetic order parameter measured at the $(0\ 2\text{–}5)_M$ peak upon warming. Error bars represent 1 standard deviation.

background measurement. The pulsed-field magnetization was calibrated using dc measurements obtained in a QD MPMS up to 7 T. The applied pulsed magnetic field was determined by the induced voltage in a coil, calibrated using the de Haas van Alphen oscillations of copper [49]. High-field torque magnetometry and resistivity measurements were carried out at National High Magnetic Field Laboratory (NHMFL) in Tallahassee. The torque was measured on a bar-shaped crystal through a CuBe cantilever beam, whose deflection was measured via capacitive techniques with a ^{3}He cryostat, and the resistivity was measured via a conventional lock-in ac technique in a 35-T resistive magnet in combination with a variable temperature insert down to 1.4 K.

III. LOW CARRIER ANTIFERROMAGNET WITH STRONG MAGNETIC ANISOTROPY

$YbRh_3Si_7$ crystallizes in the $ScRh_3Si_7$ structure type with space group $R\bar{3}c$ [20]. This structure features vertex-sharing $YbRh_6$ octahedra and Si_7 bipyramids oriented along the c axis. The details of the crystal structure of the optimally annealed crystal are presented in Fig. S1 in Ref. [40]. Because of the complexity of the rhombohedral $R\bar{3}c$ crystal structure, it will be prudent to refer to the equivalent hexagonal structure and its respective a and c crystallographic directions. The primitive rhombohedral unit cell contains two Yb atoms, while the equivalent hexagonal structure contains six Yb atoms. When working in reciprocal space, all indices are given with respect to the hexagonal reciprocal lattice. The band-structure plots adopt the rhombohedral reciprocal lattice.

We first characterize the electrical transport properties of $YbRh_3Si_7$. The $H = 0$ resistivity of the as-grown single crystals [time = 0, yellow symbols, Fig. 1(a)] shows semimetallic-like behavior as $\rho(T)$ increases upon cooling from room temperature down to $T^* \sim 15$ K, a local maximum. By contrast, the nonmagnetic analogue $LuRh_3Si_7$ is a normal metal [line, Fig. 1(a)], albeit with a relatively large resistivity of about 1 mΩ cm at 300 K. There are several plausible reasons for the observed temperature dependence of ρ in $YbRh_3Si_7$, including (i) strong hybridization between the $4f$ and conduction electron bands near the Fermi surface [50], (ii) magnetic order close to T^* in a

semimetal or semiconductor [51], or (iii) extrinsic effects, due to disorder-induced localization [52]. Annealing at fixed temperature (850 °C) with variable time (between 50 and 200 hours) allowed us to minimize disorder effects. The data in Fig. 1(a) (symbols) show a remarkable decrease of the absolute ρ values over the entire measured temperature range as the annealing time increases, favoring a picture of reduced disorder with heat treatment. This is accompanied by a decrease of residual resistivity ρ_0 with increasing annealing time, as shown in the inset of Fig. S2(a) in Ref. [40]. A Laue image of the optimally annealed crystal is shown in Fig. S2 (b). For the remainder of the paper, all data correspond to optimally annealed samples (time = 150–200 hours). While some ambiguity remains about (iii) the role of disorder-induced localization, it can be ruled out as the main cause of the $\rho(T)$ behavior in $YbRh_3Si_7$.

Scenario (ii) of magnetic order around T^* in a semimetal or semiconductor can also be ruled out: (a) T^* is field independent up to $\mu_0 H = 9$ T [Fig. 1(b)], suggesting that the peak at T^* is likely not of magnetic origin. (b) Above T^*, $\rho(T)$ does not follow an activated-type behavior, indicating that $YbRh_3Si_7$ is not a semiconductor [Fig. S3(a) in Ref. [40]]. (c) As will be shown later, magnetization, neutron diffraction, and specific heat measurements do not show any transitionlike feature at T^*. Particularly, magnetic entropy estimated from specific heat data is reduced to only 0.7 Rln2 at T^*. This is not expected in the semiconductor with magnetic order but without the Kondo effect [51]. In Sec. IV, band-structure calculations show that $YbRh_3Si_7$ is a compensated semimetal with equal hole (n_h) and electron (n_e) carrier densities. We therefore suggest that the electrical transport properties in $YbRh_3Si_7$ around T^* embody the character of a Kondo lattice, while the negative resistivity coefficient (i.e., $d\rho/dT < 0$) at high temperatures is due to spin-flip scattering of the conduction carriers off magnetic centers in a semimetallic framework. Coherence sets in at T^* and results in the drop in resistivity below this temperature [53]. Upon further cooling to the lowest temperature, the resistivity follows T^2 dependence below 2 K, indicative of Fermi liquid behavior of a strongly correlated system dictated by the Kondo effect [Fig. S2(a) in Ref. [40]]. The prefactor A in $\rho = \rho_0 + AT^2$ decreases by 1 order of magnitude from $\mu_0 H = 0$ ($A = 2.6 \times 10^{-2}$ mΩ cm K^{-2}) to $\mu_0 H = 9$ T ($A = 3.1 \times 10^{-3}$ mΩ cm K^{-2}), consistent with suppression of the Kondo effect by the magnetic field [Fig. S3(b)].

Figure 1(c) shows that the Hall coefficient R_H is positive between 300 and 10 K and strongly temperature dependent. If we assume the drift velocity of each type of carrier can be treated using the Drude model,

$$R_H = \frac{1}{|e|}\frac{(n_h\mu_h^2 - n_e\mu_e^2)}{(n_h\mu_h + n_e\mu_e)^2} > 0,$$
$$\mu_{h,e} = q\frac{\tau_{h,e}}{m_{h,e}^*},$$
$$\frac{1}{\tau_{h,e}} = \frac{1}{\tau_{ex}} + \Gamma_{h,e}, \quad (1)$$

where $\mu_{h,e}$, $\tau_{h,e}$, and $m_{h,e}^*$ are the mobility, collision time, and effective mass for holes and electrons, respectively [54]. Note that $1/\tau_{ex}$ is the rate for scattering off impurities and phonons, and $\Gamma_{h,e}$ is the rate of hole-hole (or electron-electron) intraband scattering (the interband scattering can also be absorbed into $\Gamma_{h,e}$). Since band-structure calculations (Sec. IV) show that $n_h = n_e$, the sign of R_H is determined by the difference $(\mu_h^2 - \mu_e^2)$. The observed positive R_H indicates that holes are more mobile than electrons, and this could either be due to holes being lighter or to the slowing scattering rate $\Gamma_h < \Gamma_e$, or possibly a combination of these two effects.

Magnetization, neutron diffraction, and specific heat measurements, which will be discussed below, show that $YbRh_3Si_7$ has an AFM ground state with $T_N = 7.5$ K. This is relatively high among Yb-based antiferromagnets, with very few other such systems showing comparable ordering temperatures ($Yb_3Cu_4Ge_4$ with $T_N = 7.5$ K [55], YbRhGe with $T_N = 7$ K [56], and Yb_2MgSi_2 with $T_N = 9.5$ K [57]). The $H = 0$ magnetic ordering transition is confirmed by anisotropic magnetization measurements [Fig. 1(d)]. When the magnetic field is applied parallel or perpendicular to the c axis, anisotropy is apparent in the magnetic susceptibility, with larger magnetization values along the c axis, M_c, at high temperatures indicating axial CEF anisotropy. Above 100 K, Curie-Weiss behavior is evidenced by the linear inverse magnetic susceptibility H/M [lines, Fig. 1(d)]. A linear fit of the inverse average susceptibility H/M_{ave}, where $M_{ave} = (2M_{ab} + M_c)/3$, yields an effective moment $\mu_{eff} = 4.1\ \mu_B$, close to the theoretical value for Yb^{3+} ions $\mu_{eff}^{theory} = 4.54\ \mu_B$. Upon cooling below about 10 K, a magnetic susceptibility crossover and a large (small) upturn in the M_{ab}/H (M_c/H) occur [squares (triangles) in inset, Fig. 1(d)], resembling a ferromagnetic (FM) transition with moments perpendicular to the high-T CEF axis. Ferromagnetic order along the hard axis has been observed in the heavy fermions $Yb(Rh_{0.73}Co_{0.27})_2Si_2$ [58] and $YbNi_4P_2$ [7]. The mechanism for this effect could be either quantum fluctuations or directionally dependent transverse fluctuations [59]. However, in $YbRh_3Si_7$, neutron diffraction and thermodynamic property measurements reveal that the magnetic ground state is AFM. Thus, the M/H crossover in $YbRh_3Si_7$ may have a different origin than in the above-mentioned hard-axis ferromagnets, while a minute ferromagnetic component cannot be ruled out.

To shed light on the magnetic properties of $YbRh_3Si_7$, electronic band-structure calculations were performed using the DFT and DFT + U techniques, as described in Sec. II. We have found the lowest-energy configuration to be the one in which the Yb magnetic moments are ordered ferromagnetically within the ab plane, pointing along the c axis, with AFM order between adjacent planes. Next, we present the partial DOS projected onto different orbital angular-momentum components, m_L of the Yb^{3+} ion, plotted in Fig. 1(e). Top (bottom) panels show the minority

(majority) spins, accordingly. Considering any given Yb ion, the minority-spin DOS is dominated by $m_L = 2$ (red) at the Fermi level (vertical dotted line). The other m_L orbitals, which are represented by the blue lines, lie below the Fermi level and hence do not contribute to the moment. This corresponds to the spin-orbit coupled state $|J = 7/2, m_J = 5/2\rangle$, as shown by the expression in the inset in Fig. 1(e). We conclude that the ground-state doublet is thus $|J = 7/2, m_J = 5/2\rangle$, and we expect that, under large magnetic fields, this state will become fully polarized. Accordingly, the calculated saturated moment $\mu_{\rm sat}^{\rm calc} = (L_z + 2S_z)\mu_{\rm B}/\hbar$ should be 2.86 $\mu_{\rm B}$.

We next present neutron diffraction measurements, which allow us to identify the zero field magnetic ground state of $YbRh_3Si_7$. Upon cooling below $T_{\rm N} = 7.5$ K, these measurements reveal the formation of additional Bragg reflections as shown in Fig. 1(f). These magnetic Bragg reflections were indexed with a $k = 0$ propagation vector in the $R\bar{3}c$ space group. The best agreement with the measured diffraction pattern was obtained with the Γ_5 irreducible representation, which can be written as a linear combination of two basis vectors $(3 \cdot \psi_5 + \psi_6)$ [43]. The resulting refinement is shown in Fig. 1(f). In this collinear AFM structure, the spins are constrained to lie in the *ab* plane, as represented for a single unit cell in the inset of Fig. 1(f). The ferromagnetically ordered planes are stacked antiparallel along the *c* axis. This magnetic structure has also been verified with single-crystal neutron diffraction measurements. Figure 1(g) presents the agreement between the measured and calculated structure factors. The temperature dependence of the (0, 2, −5) magnetic Bragg peak, shown in Fig. 1(h), reveals that at 4.5 K the intensity has not saturated. Thus, it is not surprising that the ordered moment determined from single-crystal diffraction, 0.36 $\mu_{\rm B}/Yb^{3+}$ at 4.5 K, is slightly smaller than the moment derived from powder diffraction, 0.47 $\mu_{\rm B}/Yb^{3+}$ at 1.5 K. This partial order parameter gives $T_{\rm N}$ around 7.5 K, in agreement with the magnetic susceptibility measurements in the inset of Fig. 1(d). It is worth highlighting that the structure determined by neutron diffraction differs from the one used in the DFT calculations; while both structures have alternating AFM coupled planes, in DFT, the moments point along the *c* axis, whereas experimentally they are found to point along the *a* axis. This discrepancy is likely due to the fact that DFT may not properly account for the crystal electric-field anisotropy. In addition, the FM-like magnetic susceptibility [inset of Fig. 1(d)] implies that the spin structure is probably noncollinear, and the net moment comes from the moment along the *a* axis. However, this net moment is most probably too small (< 0.1 $\mu_{\rm B}$) to be observable by nonpolarized neutron diffraction, so the bulk magnetization measurement does not conflict with the neutron data. The neutron data only observed the dominant magnetic phase or component.

IV. KONDO EFFECT AND HYBRIDIZATION

With the magnetic ground state resolved from neutron diffraction measurements, a better characterization of the correlations in $YbRh_3Si_7$ is needed since the $H = 0$ resistivity, shown in Fig. 1(a), hinted at possible strong correlations and Kondo screening below about 30 K. Long-range AFM order at $T_{\rm N} = 7.5$ K is marked by a broad peak in specific heat C_p [Fig. 2(a)], consistent with the magnetic susceptibility and neutron data. We define the peak temperature in $C_p(T)$ as the ordering temperature. For comparison, the specific heat data of the nonmagnetic analogue $LuRh_3Si_7$ (solid line) is also shown in Fig. 2(a). A log-log plot of $(C_p - C_n)/T$ vs T in the inset, where C_n is the nuclear contribution to the specific heat (see Fig. S4 in Ref. [40] for details), remains almost constant below 0.5 K. Then, we subtract the nonmagnetic contribution as approximated by $LuRh_3Si_7$. The resulting magnetic entropy of $YbRh_3Si_7$ amounts to only 0.37 Rln2 at $T_{\rm N}$ [Fig. 2(b)], implying strong Kondo correlations, with a Kondo temperature around 15 K determined from $S_{\rm mag}(0.5T_{\rm K}) = 0.4$ Rln2. We notice that the C_p peak around $T_{\rm N}$ is broader than that in other $4f$-based antiferromagnets. Some possibilities—including lattice defects such as mosaic grain boundaries, low-lying CEF levels, and short-range interactions above $T_{\rm N}$—may cause the rounding of the transition. First, mosaicity can be ruled out since all reflection points on the Laue image are sharp and can be mapped out by the calculated pattern [Fig. S2(b)]. Second, Fig. S5 in Ref. [40] shows that the first excited CEF level is about 26 meV, far above the measured temperature range, and hence could not cause the rounding of C_p. Finally, short-range interactions, if present, cannot be unambiguously resolved, mainly due to the fact that the small magnetic moment above $T_{\rm N}$ is close to the experimental limit of the

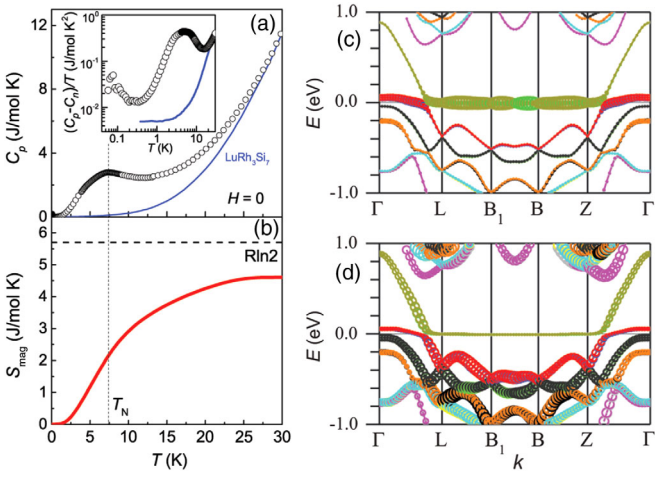

FIG. 2. (a) $H = 0$ $C_p(T)$ for $YbRh_3Si_7$ (full circles) and its nonmagnetic analogue (line) $LuRh_3Si_7$. Inset: Log-log plot of $(C_p - C_n)/T$ vs T, where C_n is the nuclear contribution to the specific heat. (b) Magnetic entropy $S_{\rm mag}(T)$. (c) Band structure of $YbRh_3Si_7$ with so-called "fat bands" highlighting the contribution from Yb f orbitals and (d) Rh and Si atoms. Thicker sections of the bands represent a larger partial contribution of the respective orbitals.

diffraction experiments. Although the exact cause of the broadening of the C_p peak is unclear at the current stage, the unusual magnetic properties of $YbRh_3Si_7$ are governed by its long-range AFM order below T_N.

To elucidate the nature of the hybridization between Yb f and conduction electron bands inferred from the thermodynamic measurements above, DFT + U calculations were performed [48] inside the AFM phase. The representative band structure is shown in Fig. 2 along the high-symmetry lines in the Brillouin zone. We have separated the partial contribution of the Yb f electrons [Fig. 2(c)] from that of the conduction electrons of Rh and Si [Fig. 2(d)] using the "fat band" representation, such that the thicker bands denote the larger contribution of the respective atomic orbitals. The results paint the canonical picture of hybridization between the very thin (atomiclike) Yb f band and the parabolic conduction band, the latter with a bandwidth on the order of 1.5 eV. The chemical potential, pinned to the Yb f level, crosses the conduction band along the Γ-Z direction, while the spectrum remains gapless (metallic in character) even in the AFM phase. The same observation is true for the paramagnetic (PM) phase (see Fig. S7 in Ref. [40]).

An additional outcome from the band-structure calculations is that there are two bands crossing the Fermi level, resulting in a compensated semimetal with an electron and hole pocket of equal volume. The DFT calculations estimate the total carrier density $n = n_h + n_e \approx 3.2 \times 10^{21}$ cm^{-3} in the PM phase and 2.9×10^{21} cm^{-3} in the AFM phase. These calculated values are close to the experimental carrier density $n_{\mathrm{exp}} \sim 1.5 \times 10^{21}$ cm^{-3} inferred from the low-temperature Hall coefficient [Fig. 1(c)] using a simplified single-band picture, where $R_H = 1/n|e|$. The presence of two bands necessitates a more detailed analysis, taking carrier mobilities into account, as in Eq. (1), but the comparison with the theory is nevertheless favorable. Of course, one must bear in mind that the DFT calculations are based on a single-particle picture and, as such, do not capture the many-body Kondo lattice phenomena. Nevertheless, the Luttinger theorem ensures us that while the quasiparticle residue and effective mass may be drastically modified due to the Kondo hybridization, the Fermi surface volume, and hence the carrier density, should remain intact. The band-structure calculations thus provide a reasonable starting point and predict the system to be a low-carrier density Kondo semimetal, in agreement with the experimental results.

V. HARD-AXIS METAMAGNETISM

Having provided evidence for the low carrier Kondo semimetal character in $YbRh_3Si_7$, we now focus on how these properties are intertwined with the even more complex magnetotransport properties when the magnetic field is orthogonal to the $H = 0$ moment direction. In the $H \| c$ field-dependent specific heat, T_N appears to be suppressed slightly by fields up to about 6 T [inset of Fig. 3(a)]. At higher fields, an additional transition becomes visible and is marked by an arrow in Fig. 3(a) for $\mu_0 H = 6.15$ T. As the field is further increased, the peak associated with this new transition becomes larger and sharper, and shifts to higher temperatures. A first-order-like transition at T = 6.8 K and $\mu_0 H = 9$ T is observed. This evolution of the transitions with applied field implies that the set of critical exponents which belongs to the magnetic universality class changes at about 6.15 T. In contrast, for $H \| ab$ [Fig. 3(b)], no additional transition is observed up to 9 T, and the $H = 0$ peak in C_p monotonically shifts to higher temperatures. This is attributed to spin fluctuations above the ordering temperatures that the magnetic field shifts the specific heat weight to higher temperatures [60]. Similar behavior has been reported in several other strongly correlated systems, such as $CeCu_{5.5}Au_{0.5}$, MnSi, and CeAuSn [61–63].

The magnetic susceptibility [Fig. 1(d)] and specific heat data [Figs. 3(a) and (b)] point to complex field-induced magnetic transitions and large CEF anisotropy in $YbRh_3Si_7$. Field-dependent thermodynamic and transport property measurements allow for an in-depth characterization of this complex magnetism. Low-temperature magnetization measurements $M(H)$ up to 7 T not only confirm the magnetic anisotropy but reveal a MM transition above $\mu_0 H = 6$ T for $H \| c$ [solid line, Fig. 3(c)]. In the orthogonal direction, no MM transition is observed [dashed line, Fig. 3(c)]. The low-field M_{ab} shows a sharp increase with H and a small hysteresis at very small fields [inset of Fig. 3(c)]. Because of the equivalence of the a and b hexagonal directions, the low field $M(H)$ behavior can be explained within a domain pinning picture because the spin configuration within the ab plane is not unique. Indeed, this magnetic structure is composed of three symmetrically equivalent domains, which can be generated from the configuration shown in Fig. 1(f) by successively rotating the spins by 120° in the ab plane. Once a field is applied within the ab plane, this symmetry is broken and the domain most closely aligned with the field will become energetically most favorable, resulting in its selection to form a single domain state. The very small, about 0.01 T, barrier to this selection and the hysteresis, of about 0.002 T, are the result of domains being pinned by the low level of disorder that is present in any material.

To investigate the evolution of M_c and temperature dependence of the MM transition at higher fields, we performed magnetization, torque, and magnetoresistance measurements up to 35 T as shown in Figs. 3(d)–3(g). All measurements were carried out for both increasing and decreasing fields, and they indicate two MM transitions, around $\mu_0 H_1 \sim 6.7$ T and $\mu_0 H_2 \sim 21$ T. The values of $\mu_0 H_1$ and $\mu_0 H_2$ were determined from the peaks or dips in the derivatives, as shown in the right axes of Figs. 3(e)–3(g). The magnetization [Fig. 3(e)] varies linearly with H up to the first critical field $\mu_0 H_1$. Following the MM transition at $\mu_0 H_1$, a linear increase of M_c is seen for fields between 10 T and 21 T, followed by

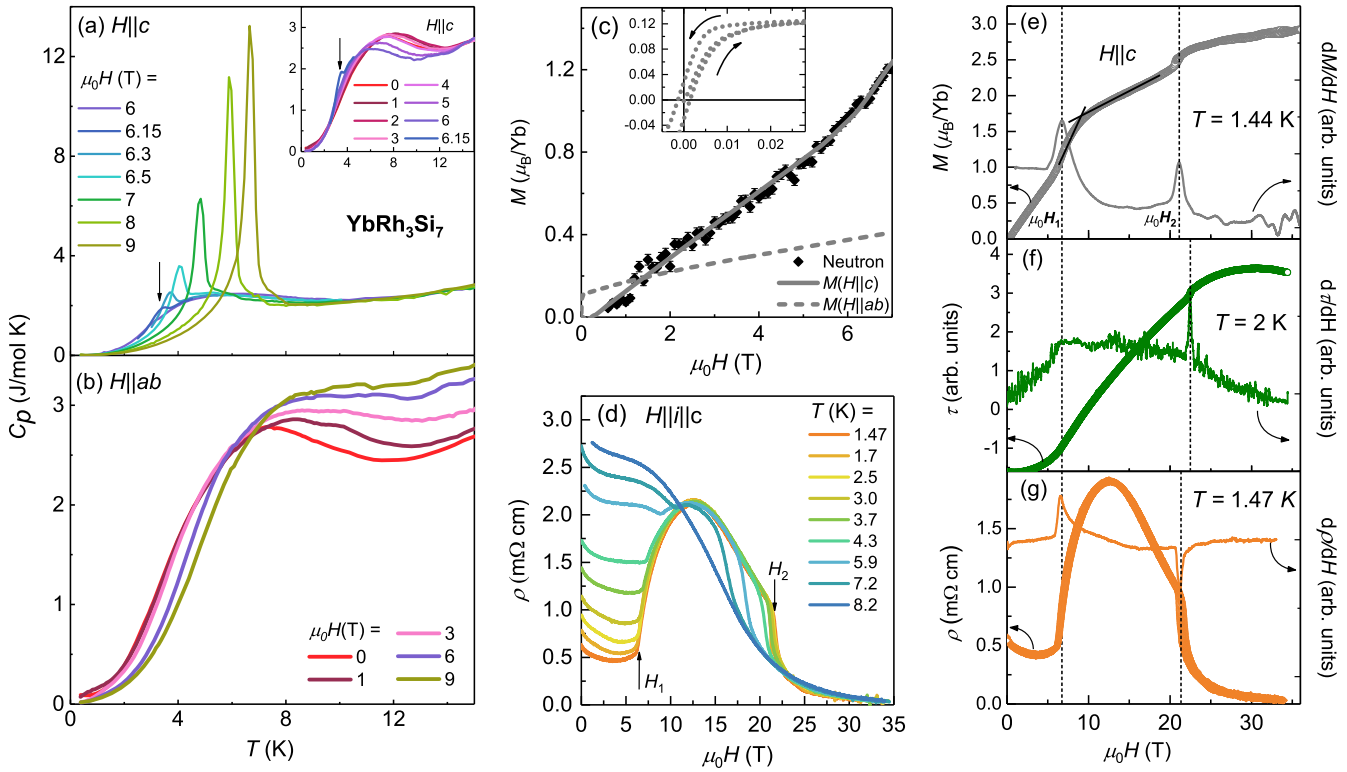

FIG. 3. (a) C_p vs T for $YbRh_3Si_7$ with magnetic fields ($\mu_0 H \geq 6$ T) applied parallel to the c axis. Inset: Low magnetic-field data ($\mu_0 H \leq 6.15$ T). (b) C_p vs T with $H||ab$. (c) M vs H at $T = 1.8$ K for $H||ab$ (dashed line) and $H||c$ (solid line) up to $\mu_0 H = 7$ T. The c-axis moment from neutron diffraction is given by the solid symbols. The inset shows the low-field data for $H||ab$. (d) $H||c$ magnetoresistance isotherms. (e)–(g) Left axis: Magnetization at $T = 1.44$ K, torque at $T = 2$ K, and resistivity at $T = 1.47$ K as a function of magnetic field $H||c$. Right axis: Derivative plots with respect to H. Dashed lines indicate the metamagnetic transitions at $\mu_0 H_1$ and $\mu_0 H_2$.

the second MM transition around $\mu_0 H_2 = 21$ T. At higher fields, the magnetization approaches a plateau close to 2.8 μ_B/Yb, much less than the Hund's rule ground-state value of 4.5 μ_B for Yb^{3+}. However, the measured value is consistent with the expected saturated magnetization for $m_j = 5/2$, which was predicted by DFT calculations to be the CEF ground state [Fig. 1(e)]. The critical fields $\mu_0 H_1$ and $\mu_0 H_2$ are also indicated by a change of slope in the magnetoresistance and torque data as shown in Figs. 3(d), 3(f), and 3(g). Temperature-dependent magnetoresistance isotherms for $H||c$ point to an increasing critical field value for $\mu_0 H_1$ and a decreasing critical field value for $\mu_0 H_2$ with increasing temperatures [Fig. 3(d)]. Across $\mu_0 H_2$, magnetization, torque, and magnetoresistance all show a hysteresis (see Fig. S8), indicating that the transition from CAFM to SPM is first order. This is in line with the sharp transition seen in C_p above $\mu_0 H = 6.5$ T [Fig. 3(a)].

VI. DISCUSSION

$YbRh_3Si_7$ is a new low carrier Kondo semimetal showing large CEF anisotropy at high temperatures and AFM order below $T_N = 7.5$ K. Zero field neutron diffraction measurements point to a collinear AFM magnetic structure, which evolves when a magnetic field is applied either parallel or perpendicular to the moments. Field-dependent magnetization measurements and theoretical calculations indicate that the phase above 20 T corresponds to the saturated $m_J = 5/2$ magnetic state. We therefore propose three distinct spin configurations to describe the different phases observed in the $H - T$ phase diagram for $H||c$ in Fig. 4. In the low field regime, from zero field up to $\mu_0 H_1$, long-range AFM order occurs, and this is schematically depicted in the bottom left plot in Fig. 4. The magnetic moments μ (red arrows) are parallel to the a axis $\mu||[100]$, with FM ab planes stacked antiferromagnetically along the c axis. In the high-field regime, $\mu_0 H \geq \mu_0 H_2$, all the moments are polarized parallel to the hexagonal c axis $\mu||[001]$, as indicated by both $M(H)$ measurements and DFT calculations. The corresponding spin-polarized paramagnetic (SPM) phase is illustrated in the bottom right plot in Fig. 4. Single-crystal neutron diffraction measurements up to $\mu_0 H||c = 8$ T do not allow us to uniquely determine the magnetic structure in the intermediate phase. However, the c-axis ordered moment measured on the (110) Bragg peak is consistent with magnetization measurements, as shown in Fig. 3(c). Above $\mu_0 H_1$, we do not observe the formation of any new magnetic Bragg peaks, as would be

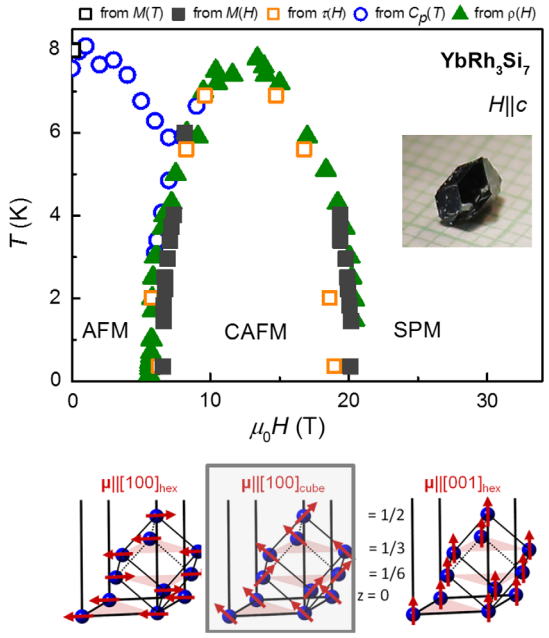

FIG. 4. $T-H$ phase diagram of $YbRh_3Si_7$ together with three distinct magnetic spin configurations in different magnetic-field regions. A picture of the crystal is shown in the inset.

expected for an MM transition to a complex conical or helical state. Instead, we observe a sudden increase in the $k=0$ FM moment. Thus, we propose a simple effective spin configuration for the intermediate phase that is consistent with our neutron diffraction measurements and can quantitatively describe the isothermal magnetization. The system enters a canted antiferromagnetic (CAFM) state, with the moments aligned along the nearest-neighbor direction in the distorted cubic Yb sublattice, which is around a 45-degree angle with the hexagonal axes (Fig. 4, bottom middle). The $H\|[001]$ component of the magnetization for such a CAFM spin configuration can be calculated from $M_{001}=\mu\cos\theta=2.86\times(3.304\text{Å}/5.468\text{Å})\ \mu_B/\text{Yb}=1.73\ \mu_B/\text{Yb}$ (schematically shown in Fig. S9 in Ref. [40]). This value agrees well with the measured low-T magnetization around 9 T, $M_c(9\text{ T};1.44\text{ K})\sim 1.7\ \mu_B/\text{Yb}$, indicated by the intersection of two black lines [Fig. 3(e)].

From neutron diffraction determination of the AFM structure, we know that the magnetic ordered moments are in the ab plane and that they order antiferromagnetically along the c axis. In this magnetic structure arrangement, one would expect that a c-axis aligned magnetic field should gradually polarize the moment along the c axis as a function of increasing magnetic field. This is because a c-axis aligned field is already in a direction perpendicular to the in-plane moment, and this should not induce an additional spin-flop transition. For an in-plane aligned field, one would expect a spin-flop transition to occur above a critical field so that the AFM order moment will align perpendicular to the applied field direction. When the spin-flop transition occurs, we would expect sudden changes in magnetization and large magnetoresistance, as seen in the case of YbAgGe [27] and $YbIr_2Zn_{20}$ [37]. Our observation in $YbRh_3Si_7$ is contrary to this expectation. For a field in the ab plane, we see no field-induced spin-flop transition and very little increase in the total magnetization. On the other hand, we see clear c-axis field-induced magnetization and a specific heat anomaly as a function of increasing field. This means that the 7-T in-plane field we applied was unable to drive the system into a CAFM state, while the same field along the c axis can dramatically affect the long-range AFM order and drives the system into a FM state in a staged fashion, completely unexpected given the AFM arrangements of the spins in the system.

The MM transitions in $YbRh_3Si_7$ are genuine phase transitions instead of crossovers, in contrast to some other metamagnetic systems [29,32,33]. Similar phase diagrams with multiple MM transitions have been reported in other Ce- or Yb-based compounds, such as $YbNiSi_3$ [25,64], YbAgGe [65,66], $CeAgBi_2$ [67], and $CeAuSb_2$ [68]. However, as discussed, the MM transitions in these compounds occur for magnetic fields parallel to the $H=0$ moment direction (M_0). Remarkably, in $YbRh_3Si_7$, the MM transitions occur at lower fields for $H\perp M_0$. This is first apparent in the anisotropic $M(H)$ isotherms [Fig. 3(c)], with angle-dependent magnetoresistance data reinforcing this point, as H is rotated away from the c axis towards the ab plane (Fig. S10 in Ref. [40]). To our knowledge, $YbRh_3Si_7$ is therefore the only Ce- or Yb-based compound to show MM transitions for $H\perp M_0$, rendering the competition between the different energy scales (RKKY, CEF, Kondo, etc.) particularly complex. As DFT calculations already suggested, the energy scales for the moment parallel to the a and c axes might be very close, and a modest magnetic field is sufficient to reorient the magnetic moment direction. This suggestion is supported by the isothermal magnetization data, where a crossover of M_c and M_{ab} is observed around 1.6 T, as shown in Fig. 3(c). When the applied field is larger than 1.6 T, the CEF easy-axis anisotropy dominates and no crossover is expected, in contrast to the low field data shown in the inset of Fig. 1(d). This is likely the result of field tuning of direct competition between the single-ion CEF anisotropy and anisotropic exchange interactions, with the former dictating a magnetic easy axis parallel to the c axis and the latter leading to the low field moment alignment in the ab plane. However, this competition alone cannot explain the abrupt increase in resistivity that occurs at the onset of the MM transition at μ_0H_1 [Fig. 3(g)]. In addition, in angle-dependent magnetoresistivity measurements (Fig. S10), as the magnetic field is rotated away from the c axis, a monotonic increase of μ_0H_1 and a monotonic decrease of resistance are observed, instead of extremes around $\theta=45$ degrees, i.e., the lowest energy state in the CAFM phase. There are some other possible underlying energy scales that are not discussed in

this study, including (1) a structural transition with field or (2) a Kondo breakdown scenario where the itinerant $4f$ electrons become localized at the MM transitions [69]. The understanding of the exact nature of the anomalous metamagnetism in $YbRh_3Si_7$ warrants further study.

In summary, $YbRh_3Si_7$ is a new low carrier, antiferromagnetic, Kondo lattice compound with anomalous metamagnetism. It serves as a forerunner among Ce- and Yb-based 1-3-7 analogues, rendering the 1-3-7 structure an ideal host structure to investigate the intertwinement of multiple energy scales, including RKKY, Kondo, CEF anisotropy, and anisotropic exchange interactions.

ACKNOWLEDGMENTS

We thank P. Canfield, G. Lapertot, F. Steglich, C. Batista, L. Balents, and Q. Si for fruitful discussions. B. K. R., M. S., C. L. H., and E. M. acknowledge support from the Gordon and Betty Moore Foundation EPiQS initiative through Grant No. GBMF4417. The work at University of Texas at Dallas was supported by Grant No. NSF-DMR-1700030. The scientific work at LANL was funded by the LDRD program and by the DOE BES FWP "Science in 100 T". This research used resources at the High Flux Isotope Reactor, a DOE Office of Science User Facility operated by the Oak Ridge National Laboratory. The N. H. M. F. L. acknowledges support from the U.S. NSF Cooperative Grants No. DMR1157490 and No. DMR-1644779, the U.S. DOE, and the State of Florida. L. B. is supported by DOE-BES through Grant No. DE-SC0002613. P. D. acknowledges support from the U.S. DOE, BES DE-SC0012311, and the Robert A. Welch Foundation Grant No. C-1839. A. H. N. and V. L. acknowledge the support of the Robert A. Welch Foundation Grant No. C-1818. A. H. N. was also supported by the U.S. NSF Grant No. DMR-1350237. Computational resources at Rice University were provided by the Big-Data Private-Cloud Research Cyberinfrastructure MRI award funded by NSF under Grant No. CNS-1338099. The identification of any commercial product or tradename does not imply endorsement or recommendation by the National Institute of Standards and Technology.

[1] H. v. Löhneysen, A. Rosch, M. Vojta, and P. Wöfle, *Fermi-Liquid Instabilities at Magnetic Quantum Phase Transitions*, Rev. Mod. Phys. **79**, 1015 (2007).

[2] E. Schuberth, M. Tippmann, L. Steinke, S. Lausberg, A. Steppke, M. Brando, C. Krellner, C. Geibel, R. Yu, Q. Si, and F. Steglich, *Emergence of Superconductivity in the Canonical Heavy-Electron Metal* $YbRh_2Si_2$, Science **351**, 485 (2016).

[3] J. Paglione, T. A. Sayles, P.-C. Ho, J. R. Jeffries, and M. B. Maple, *Incoherent Non-Fermi-Liquid Scattering in a Kondo Lattice*, Nat. Phys. **3**, 703 (2007).

[4] J. A. Mydosh and P. M. Oppeneer, *Hidden Order Behaviour in* URu_2Si_2 *(A Critical Review of the Status of Hidden Order in 2014)*, Philos. Mag. **94**, 3642 (2014).

[5] D. Gignoux and D. Schmitt, *Frustration in Rare Earth Intermetallic Compounds*, J. Alloys Compd. **326**, 143 (2001).

[6] J. Custers, P. Gegenwart, H. Wilhelm, K. Neumaier, Y. Tokiwa, O. Trovarelli, C. Geibel, F. Steglich, C. Pépin, and P. Coleman, *The Break-up of Heavy Electrons at a Quantum Critical Point*, Nature (London) **424**, 524 (2003).

[7] A. Steppke, R. Küchler, S. Lausberg, E. Lengyel, L. Steinke, R. Borth, T. Lühmann, C. Krellner, M. Nicklas, C. Geibel, F. Steglich, and M. Brando, *Ferromagnetic Quantum Critical Point in the Heavy-Fermion Metal* $YbNi_4(P_{1-x}As_x)_2$, Science **339**, 933 (2013).

[8] T. T. M. Palstra, A. A. Menovsky, J. van den Berg, A. J. Dirkmaat, P. H. Kes, G. J. Nieuwenhuys, and J. A. Mydosh, *Superconducting and Magnetic Transitions in the Heavy-Fermion System* URu_2Si_2, Phys. Rev. Lett. **55**, 2727 (1985).

[9] B. K. Rai, I. W. H. Oswald, J. Y. Chan, and E. Morosan, *Intermediate Valence to Heavy Fermion through a Quantum Phase Transition in* $Yb_3(Rh_{1-x}T_x)_4Ge_13$ *(*$T = Co, Ir$*) Single Crystals*, Phys. Rev. B **93**, 035101 (2016).

[10] Y. Aoki, T. D. Matsuda, H. Sugawara, H. Sato, H. Ohkuni, R. Settai, Y. Ōnuki, E. Yamamoto, Y. Haga, A. V. Andreev, V. Sechovsky, L. Havela, H. Ikeda, and K. Miyake, *Thermal Properties of Metamagnetic Transition in Heavy-Fermion Systems*, J. Magn. Magn. Mater. **177–181**, 271 (1998) and references therein.

[11] K. Prokes, M. I. Bartashevich, T. Goto, H. Nakotte, E. G. Haanappel, A. Syshchenko, F. R. de Boer, A. Lacerda, L. C. J. Perreira, and V. Sechovsky, *Metamagnetic Transition in* U_2Pd_2In, Physica B (Amsterdam) **294**, 288 (2001).

[12] K. Sugiyama, T. IIZuka, D. Aoki, Y. Tokiwa, K. Miyake, N. Watanabe, K. Kindo, T. Inoue, E. Yamamoto, Y. Haga, and Y. Ōnuki, *High-Field Magnetization of* USn_3 *and* UPb_3, J. Phys. Soc. Jpn. **71**, 326 (2002).

[13] C. Capan, A. Bianchi, F. Ronning, A. Lacerda, J. D. Thompson, M. F. Hundley, P. G. Pagliuso, J. L. Sarrao, and R. Movshovich, *Non-Fermi-Liquid Behavior in* $CeIrIn_5$ *Near a Metamagnetic Transition*, Phys. Rev. B **70**, 180502(R) (2004).

[14] L. Balicas, S. Nakatsuji, H. Lee, P. Schlottmann, T. P. Murphy, and Z. Fisk, *Magnetic Field-Tuned Quantum Critical Point in* $CeAuSb_2$, Phys. Rev. B **72**, 064422 (2005).

[15] E. Morosan, S. L. Budko, and P. C. Canfield, *Angular-Dependent Planar Metamagnetism in the Hexagonal Compounds* TbPtIn *and* TmAgGe, Phys. Rev. B **71**, 014445 (2005).

[16] G. M. Schmiedeshoff, E. D. Mun, A. W. Lounsbury, S. J. Tracy, E. C. Palm, S. T. Hannahs, J.-H. Park, T. P. Murphy, S. L. Budko, and P. C. Canfield, *Multiple Regions of Quantum Criticality in* YbAgGe, Phys. Rev. B **83**, 180408(R) (2011).

[17] M. Deppe, S. Lausberg, F. Weickert, M. Brando, Y. Skourski, N. Caroca-Canales, C. Geibel, and F. Steglich, *Pronounced First-Order Metamagnetic Transition in the Paramagnetic Heavy-Fermion System* CeTiGe, Phys. Rev. B **85**, 060401(R) (2012).

[18] S. Lucas, K. Grube, C.-L. Huang, A. Sakai, S. Wunderlich, E. L. Green, J. Wosnitza, V. Fritsch, P. Gegenwart, O. Stockert, and H. v. Löhneysen, *Entropy Evolution in the Magnetic Phases of Partially Frustrated* CePdAl, Phys. Rev. Lett. **118**, 107204 (2017).

[19] S. A. Grigera, P. Gegenwart, R. A. Borzi, F. Weickert, A. J. Schofield, R. S. Perry, T. Tayama, T. Sakakibara, Y. Maeno, A. G. Green, and A. P. Mackenzie, *Disorder-Sensitive Phase Formation Linked to Metamagnetic Quantum Criticality*, Science **306**, 1154 (2004).

[20] B. Chabot, N. Engel, and E. Parthé, *Trirhodium Scandium Heptasilicide and Triiridium Scandium Heptasilicide with a New Rhombohedral Structure Type*, Acta Crystallogr. Sect. B **37**, 671 (1981).

[21] P. Lorenz and W. Jung, $MgIr_3Si_7$, *a New Magnesium Iridium Silicide with the* $ScRh_3Si_7$ *Type Structure*, Acta Crystallogr. Sect. E **62**, i173 (2006).

[22] S. E. Latturner, D. Bilc, J. R. Ireland, C. R. Kannewurf, S. D. Mahanti, and M. G. Kanatzidis, $REAu_3Al_7$ *(*RE = Rare Earth*): New Ternary Aluminides Grown from Aluminum Flux*, J. Solid State Chem. **170**, 48 (2003).

[23] M. Falmbigl, F. Kneidinger, A. Grytsiv, H. Michor, H. Müller, P. Rogl, E. Bauer, G. Hilscher, and G. Giester, *Crystal Structure, and Physical Properties of the Novel Compounds* $EuRh_3Ge_7$ *and* $EuIr_3Ge_7$, Intermetallics **42**, 45 (2013).

[24] G. Cordier and C. Dietrich, *Crystal Structure of Ytterbium Gold Gallium,* $YbAu_3Ga_7$ *in the* $ScRh_3Si_7$*-type*, Z. Kristallogr. **211**, 118 (2013).

[25] S. L. Budko, P. C. Canfield, M. A. Avila, and T. Takabatake, *Magnetic-Field Tuning of the Low-Temperature State of* $YbNiSi_3$, Phys. Rev. B **75**, 094433 (2007).

[26] Y. Hirose, M. Toda, S. Yoshiuchi, S. Yasui, K. Sugiyama, F. Honda, M. Hagiwara, K. Kindo, R. Settai, and Y. Ōnuki, *Metamagnetic Transition in Heavy Fermion Compounds* YbT_2Zn_{20} *(*T : Co, Rh, Ir*)*, J. Phys. Conf. Ser. **273**, 012003 (2011).

[27] S. L. Budko, E. Morosan, and P. C. Canfield, *Magnetic Field Induced Non-Fermi-Liquid Behavior in* YbAgGe *Single Crystals*, Phys. Rev. B **69**, 014415 (2004).

[28] K. Matsubayashi, T. Hirayama, T. Yamashita, S. Ohara, N. Kawamura, M. Mizumaki, N. Ishimatsu, S. Watanabe, K. Kitagawa, and Y. Uwatoko, *Pressure-Induced Valence Crossover and Novel Metamagnetic Behavior near the Antiferromagnetic Quantum Phase Transition of* $YbNi_3Ga_9$, Phys. Rev. Lett. **114**, 086401 (2015).

[29] A. Miyake, Y. Sato, M. Tokunaga, J. Jatmika, and T. Ebihara, *Different Metamagnetism between Paramagnetic* Ce *and* Yb *Isomorphs*, Phys. Rev. B **96**, 085127 (2017).

[30] H. Sugawara, Y. Aoki, H. Sato, N. Mushnikov, and T. Goto, *New Heavy Fermion Metamagnet* $CeFe_2Ge_2$, J. Phys. Soc. Jpn. **68**, 1094 (1999).

[31] J. Flouquet, P. Haen, S. Raymond, D. Aoki, and G. Knebel, *Itinerant Metamagnetism of* $CeRu_2Si_2$*: Bringing out the Dead. Comparison with the New* $Sr_3Ru_2O_7$ *Case*, Physica B (Amsterdam) **319**, 251 (2002).

[32] D. Aoki, C. Paulsen, T. D. Matsuda, L. Malone, G. Knebel, P. Lejay, R. Settai, Y. Ōnuki, and J. Flouquet, *Pressure Evolution of the Magnetic Field induced Ferromagnetic Fluctuation through the Pseudo-Metamagnetism of* $CeRu_2Si_2$, J. Phys. Soc. Jpn. **80**, 053702 (2011).

[33] Y. Tokiwa, C. Stingl, M.-S. Kim, T. Takabatake, and P. Gegenwart, *Characteristic Signatures of Quantum Criticality Driven by Geometrical Frustration*, Sci. Adv. **1**, e1500001 (2015).

[34] N. Tsujii, L. Keller, A. Dönni, and H. Kitazawa, *Anisotropic Magnetic Properties and Magnetic Structure of* YbPdSi, J. Phys. Condens. Matter **28**, 336002 (2016).

[35] K. Iwakawa, Y. Hirose, K. Enoki, K. Sugiyama, T. Takeuchi, F. Honda, M. Hagiwara, K. Kindo, T. Nakano, Y. Nozue, R. Settai, and Y. Onuki, *Multiple Metamagnetic Transitions in Antiferromagnet* Yb_2Pt_2Pb *with the Shastry-Sutherland Lattice*, J. Phys. Soc. Jpn. **81**, SB058 (2012).

[36] T. Yamashita, S. Ohara, and I. Sakamoto, *Magnetic Properties of Two-Dimensional Honeycomb Lattice Magnet* RNi_3Al_9 *(*R = Gd *to Lu)*, J. Phys. Soc. Jpn. **80**, SA080 (2011).

[37] T. Takeuchi, S. Yasui, M. Toda, M. Matsushita, S. Yoshiuchi, M. Ohya, K. Katayama, Y. Hirose, N. Yoshitani, F. Honda, K. Sugiyama, M. Hagiwara, K. Kindo, E. Yamamoto, Y. Haga, T. Tanaka, Y. Kubo, R. Settai, and Y. Onuki, *Metamagnetic Behavior in Heavy-Fermion Compound* $YbIr_2Zn_{20}$, J. Phys. Soc. Jpn. **79**, 064609 (2010).

[38] G. M. Sheldrick, *SHELX-2013-Programs for Crystal Structure Analysis: I. Structure Determination (SHELXS) and II. Refinement (SHELXL-2013)*, (University of Gottingen, Germany, 2013).

[39] G. M. Sheldrick, *SHELXT Integrated Space-Group and Crystal-Structure Determination*, Acta Crystallogr. Sect. A **71**, 3 (2015).

[40] See Supplemental Material at http://link.aps.org/supplemental/10.1103/PhysRevX.8.041047 for details of crystallographic analysis, the low-temperature resistivity data, the Laue picture of an optimally annealed crystal, analysis of nuclear contribution to the specific heat, inelastic neutron scattering data, band structural calculations, torque data at 0.35 K, the schematic view of CAFM phase, and angular dependent magnetoresistance data.

[41] J. W. Lynn, Y. Chen, S. Chang, Y. Zhao, S. Chi, W. Ratcliff II, B. G. Ueland, and R. W. Erwin, *Double-Focusing Thermal Triple-Axis Spectrometer at the NCNR*, J. Res. Natl. Inst. Stand. Technol. **117**, 61 (2012).

[42] B. C. Chakoumakos, H. B. Cao, F. Ye, A. D. Stoica, M. Popovici, M. Sundaram, W. Zhou, J. S. Hicks, G. W. Lynn, and R. A. Riedel, *Four-Circle Single-Crystal Neutron Diffractometer at the High Flux Isotope Reactor*, J. Appl. Crystallogr. **44**, 655 (2011).

[43] A. S. Wills, *A New Protocol for the Determination of Magnetic Structures Using Simulated Annealing and Representational Analysis (SARAh)*, Physica B (Amsterdam) **276–278**, 680 (2000).

[44] J. Rodriguez-Carvajal, *Recent Advances in Magnetic Structure Determination by Neutron Powder Diffraction*, Physica B (Amsterdam) **192**, 55 (1993).

[45] P. Dai *et al.*, 1810755, STFC ISIS Facility, doi:10.5286/ISIS.E.92919679.

[46] P. Blaha, K. Schwarz, G. Madsen, D. Kvasnicka, and J. Luitz, *An Augmented Plane Wave+Local Orbitals Program*

for Calculating Crystal Properties (Vienna University of Technology, Vienna, Austria, 2001).

[47] J. P. Perdew, K. Burke, and M. Ernzerhof, *Generalized Gradient Approximation Made Simple*, Phys. Rev. Lett. **77**, 3865 (1996).

[48] V. I. Anisimov, I. V. Solovyev, M. A. Korotin, M. T. Czyzyk, and G. A. Sawatzky, *Density-Functional Theory and NiO Photoemission Spectra*, Phys. Rev. B **48**, 16929 (1993).

[49] P. A. Goddard, J. Singleton, P. Sengupta, R. D. McDonald, T. Lancaster, S. J. Blundell, F. L. Pratt, S. Cox, N. Harrison, J. L. Manson, H. I. Southerland, and J. A. Schleuter, *Experimentally Determining the Exchange Parameters of Quasi-Two-Dimensional Heisenberg Magnets*, New J. Phys. **10**, 083025 (2008).

[50] M. Dzero, K. Sun, V. Galitski, and P. Coleman, *Topological Kondo Insulators*, Phys. Rev. Lett. **104**, 106408 (2010).

[51] P. Wachter, L. Degiorgi, G. Wetzel, H. Schwer, K. Mattenberger, T. Herrmannsdorfer, and P. Fischer, $Ce_3Cu_3Sb_4$ *: A Canted Antiferromagnetic Semimetal*, Acta Phys. Pol. A **97**, 43 (2000).

[52] P. W. Anderson, *Absence of Diffusion in Certain Random Lattices*, Phys. Rev. **109**, 1492 (1958).

[53] M. Lavagna, C. Lacroix, and M. Cyrot, *Resistivity of the Kondo Lattice*, J. Phys. F **12**, 745 (1982).

[54] N. W. Ashcroft and N. D. Mermin, *Solid State Physics* (Holt, Rienhart and Winston, California, 1976).

[55] S. K. Dhar, S. Singh, P. Bonville, C. Mazumdar, P. Manfrinetti, and A. Palenzona, *Magnetic Behavior of* $Yb_3Cu_4Ge_4$ *and* $Gd_3Cu_4Ge_4$, Physica B (Amsterdam) **312–313**, 846 (2002).

[56] K. Katoh, Y. Mano, K. Nakano, G. Terui, Y. Niide, and A. Ochiai, *Magnetic Properties of* YbTGe *(*T = Rh, Cu, Ag*)*, J. Magn. Magn. Mater. **268**, 212 (2004).

[57] K. V. Shah, P. Bonville, P. Manfrinetti, F. Wrubl, and S. K. Dhar, *The* $Yb_2Al_{1-x}Mg_xSi_2$ *Series from a Spin Fluctuation* $(x = 0)$ *to a Magnetically Ordered Ground State* $(x = 1)$, J. Phys. Condens. Matter **21**, 176001 (2009).

[58] E. C. Andrade, M. Brando, C. Geibel, and M. Vojta, *Competing Orders, Competing Anisotropies, and Multicriticality: The Case of Co-doped* $YbRh_2Si_2$, Phys. Rev. B **90**, 075138 (2014).

[59] F. Krüger, C. J. Pedder, and A. G. Green, *Fluctuation-Driven Magnetic Hard-Axis Ordering in Metallic Ferromagnets*, Phys. Rev. Lett. **113**, 147001 (2014).

[60] D. Vollhardt, *Characteristic Crossing Points in Specific Heat Curves of Correlated Systems*, Phys. Rev. Lett. **78**, 1307 (1997).

[61] H. G. Schlager, A. Schröder, M. Welsch, and H. v. Löhneysen, *Magnetic Ordering in* $CeCu_{6-x}Au_x$ *Single Crystals: Thermodynamic and Transport Properties*, J. Low Temp. Phys. **90**, 181 (1993).

[62] M. Janoschek, M. Garst, A. Bauer, P. Krautscheid, R. Georgii, P. Böni, and C. Pfleiderer, *Fluctuation-Induced First-Order Phase Transition in Dzyaloshinskii-Moriya Helimagnets*, Phys. Rev. B **87**, 134407 (2013).

[63] C. L. Huang, V. Fritsch, B. Pilawa, C. C. Yang, M. Merz, and H. v. Löhneysen, *Low-Temperature Magnetic, Thermodynamic, and Transport Properties of Antiferromagnetic* CeAuSn *Single Crystals*, Phys. Rev. B **91**, 144413 (2015).

[64] Y. Kobayashi, T. Onimaru, M. A. Avila, K. Sasai, M. Soda, K. Hirota, and T. Takabatake, *Neutron Scattering Study of Kondo Lattice Antiferromagnet* $YbNiSi_3$, J. Phys. Soc. Jpn. **77**, 124701 (2008).

[65] Y. Tokiwa, M. Garst, P. Gegenwart, S. L. Bud'ko, and P. C. Canfield, *Quantum Bicriticality in the Heavy-Fermion Metamagnet* YbAgGe, Phys. Rev. Lett. **111**, 116401 (2013).

[66] B. Fåk, D. F. McMorrow, P. G. Niklwotz, S. Raymond, E. Ressouche, J. Flouquet, P. C. Canfield, S. L. Bud'ko, Y. Janssen, and M. J. Gutmann, *An Inelastic Neutron Scattering Study of Single-Crystal Heavy-Fermion* YbAgGe, J. Phys. Condens. Matter **17**, 301 (2005).

[67] S. M. Thomas, P. F. S. Rosa, S. B. Lee, S. A. Parameswaran, Z. Fisk, and J. Xia, *Hall Effect Anomaly and Low-Temperature Metamagnetism in the Kondo Compound* $CeAgBi_2$, Phys. Rev. B **93**, 075149 (2016).

[68] G. G. Marcus, D.-J. Kim, J. A. Tutmaher, J. A. Rodriguez-Rivera, J. O. Birk, C. Niedermeyer, H. Lee, Z. Fisk, and C. L. Broholm, *Multi-q Mesoscale Magnetism in* $CeAuSb_2$, Phys. Rev. Lett. **120**, 097201 (2018).

[69] S. V. Kusminskiy, K. S. D. Beach, A. H. C. Neto, and D. K. Campbell, *Mean-Field Study of the Heavy-Fermion Metamagnetic Transition*, Phys. Rev. B **77**, 094419 (2008).